

Received May 13, 2019, accepted June 9, 2019, date of publication June 13, 2019, date of current version June 24, 2019.

Digital Object Identifier 10.1109/ACCESS.2019.2922422

# Negative Group Delay Theory of a Four-Port RC-Network Feedback Operational Amplifier

FAYU WAN<sup>1</sup>, (Member, IEEE), TAOCHENG GU<sup>1</sup>, BLAISE RAVELO<sup>1</sup>, (Member, IEEE), BINHONG LI<sup>2</sup>, JING CHENG<sup>3</sup>, QINGYUN YUAN<sup>4</sup>, AND JUNXIANG GE<sup>1</sup>

<sup>1</sup>Nanjing University of Information Science and Technology, Nanjing 210044, China

<sup>2</sup>Key Laboratory of Silicon Device Technology, Chinese Academy of Sciences, Beijing, China

<sup>3</sup>Anhui Agricultural University, College of Science, Hefei, China

<sup>4</sup>National Key Laboratory of Electromagnetic Environment Effect, Army Engineering University of PLA, Shijiazhuang, China

Corresponding author: Binhong Li (libinhong@ime.ac.cn)

This work was supported in part by NSFC under Grant 61601233 and Grant 61750110535, in part by the Electrostatic Research Foundation of Liu Shanghe Academicians and Experts Workstation, Beijing Orient Institute of Measurement and Test under Grant BOIMTLSHJD20181003, in part by NSF of Jiangsu under Grant BK20150918, in part by the Jiangsu Innovation and Enterprise Group Talents Plan 2015 under Grant SRCB201526, and in part by PAPD.

**ABSTRACT** An innovative negative group delay (NGD) theory based on a unity direct chain feedback (UDCF) circuit topology is developed in this paper. This NGD circuit is an active cell constituted by an operational amplifier in feedback with a four-port RC-network. This NGD circuit theory is developed based on the S-parameter model analytically established from the equivalent impedance matrix. The UDCF group delay frequency response is expressed as a function of the feedback RC-cell and the operational amplifier parameters. The NGD analysis of the developed UDCF cell is introduced. According to theoretical analysis, under a certain condition, the UDCF topology is susceptible to behave as a low-pass NGD function. The UDCF cell NGD characteristics are defined theoretically. The theoretical prediction is verified numerically and experimentally in both the frequency- and time-domain by designing and fabricating an active PCB prototype. The simulations and experimentations show that the UDCF circuit exhibits an NGD of approximately -38 ns with NGD cut-off frequency of about 5.5 MHz. More importantly, it is demonstrated in the time-domain that the low-pass NGD effect enables the UDCF cell to generate advanced output with sinc waveform input voltages.

**INDEX TERMS** Circuit theory, negative group delay (NGD), active topology, S-parameter modeling, time-domain demonstration, unit direct chain feedback (UDCF).

## I. INTRODUCTION

The performance of modern electronic circuits and systems depends implicitly on the operating signal delay. The detrimental effect of undesirable signal delays can be encountered in different electronic devices [1]–[3]. The time delay may affect globally both discrete time and time varying system globally performances. In a recent study, a prediction scheme for input delay was investigated [4]. In addition, a condition of linear system stability was established as a function of the dwell-time parameters [5].

Signal latencies constitute key elements during the design cycle and the fabrication process of electronic and electrical engineering systems. Different modules of the time-delay

function can be found at various levels of engineering systems. For example, time-delay systems were implemented to control the time lags used in vibrational feedback control [6]. An improved stabilization method dedicated to typically linear systems with time delay was reported in [7]. Subsequently, a delay-dependent H-infinity control of linear descriptor systems was introduced [8]. Delay-dependent criteria were found to be required for robust stability analysis [9]. According to the study reported in [10] that the problem of time-delay systems stability may involve an integral inequality. Therefore, the development of innovative methods for time-delay systems remains a desired goal for automatic and electronic design engineers as well as simulation engineers.

Signal propagation and group delays remain limiting factors for circuit operation speed for passive or active

The associate editor coordinating the review of this manuscript and approving it for publication was Yingsong Li.

systems [11]. In addition to the undesirable noise issues, group delay effects degrade the radio frequency (RF) electronic device performances [12]. Approximations of all-pass time-delay meant for RF analog filters were introduced in [13]. Generally, techniques to alleviate these effects use positive time or group delay. However, a technique based on negative group delay (NGD) has also been developed [14]. This counterintuitive technique consists of signal delay cancellation based on the NGD of low frequency amplifiers.

Note that NGD phenomena are not contradictory but are in fact required by causality [15], [16]. In addition, the existence of the NGD phenomenon has been demonstrated with the occurrence of signal advance [17], [18]. An NGD passive circuit was incorporated with a resonant filter function analytically related to the absorption effect [19]. Furthermore, the NGD phenomenon was observed with audio signals in low frequency circuits [20] and within a photonic crystal structure [21]. Based on the NGD effect, a system for real-time signal prediction has been proposed [22], [23] and hypothesized to be of relevance in neural computation in general [24] and in the human motor control system in particular [25]. It stands to reason that the utilization of NGD in applications has limits, for example, limits due to instabilities and long transients in linear systems [26], [27] and inherent losses in passive circuits [28]–[30]. To overcome the latter effect, active circuit topologies based on the use of RF/microwave field effect transistors (FETs) [31] and low noise amplifiers (LNAs) [32], [33] have been developed recently [31]. To broaden the use of NGD function to electronics and electrical design engineers, nonconventional circuit theory for which the NGD behaviors are similar to the linear filter gain was investigated in [31] and [34]. This similarity pedagogically the way towards practice of NGD engineering by future engineers. The analogy between NGD and filter response is prominent to the possibility of NGD function implementations in electrical and other systems.

Nonetheless, RF transistor-based NGD circuits do not operate efficiently with the DC component of baseband signals. As a result, in the present paper, an innovative NGD theory of RC-network and operational amplifier-based topology is proposed. Using the proposed approach, the designability of operational amplifier based Low-pass NGD topology to operate in Mega-Hertz RF frequencies is demonstrated both theoretically and experimentally in the frequency-domain and the time-domain. In this paper, the NGD theory of an innovative active circuit topology is investigated. The paper is focused on the analysis and synthesis of a typical low-pass NGD topology. In difference with the previous works proposed in [33]–[36]:

- The NGD topology developed in the present paper involves a four-port passive RC-network in feedback with an operational amplifier compared to a simple two-port network for the topology introduced in [36].

- The NGD theory developed in the present paper is constructed with the two-port S-parameter model, while paper [36] is simply base on the voltage transfer function. The analytical expressions of reflection and transmission coefficients are established. The NGD analysis is established with the group delay from the transmission coefficient in function of the passive feedback circuit and the operational amplifier parameters.
- The NGD analysis includes the stability aspect in function of the feedback circuit parameters. This stability analysis is never being done before based on the authors best knowledge.
- And the NGD analysis introduced in paper [36] is only limited to the frequency domain simulations. However, the present paper proposed more complete study including both the frequency and time domain simulation and measurement results.

The paper is divided into three sections. Section II describes the theoretical analysis based on S-parameter modeling and establishes the NGD characteristics from the S-matrix elaboration. Different from the all previous NGD theories [14]–[36], to the best of the authors' knowledge, the analytical formulation in this paper regarding the stability of NGD feedback circuit is unique. Section III considers numerical parametric analyses and experimental validations. Parametric analyses based on numerical modeling will be compared with theoretical calculations. The proof-of-concept (POC) printed circuit board (PCB) is fabricated as an NGD circuit prototype and then, experimental validations in the frequency-domain and the time-domain are discussed. Section IV provides a discussion of the results and the conclusion.

## II. THEORETICAL INVESTIGATION OF THE PROPOSED UNITY DIRECT CHAIN FEEDBACK (UDCF) TOPOLOGY

The present section is focused on the theoretical concept involving the NGD cell constituting the UDCF topology. In this section, the S-parameter model is developed, the NGD analysis and characterization are introduced, and the synthesis method as a function of the NGD circuit specifications is derived.

### A. THEORY OF THE UDCF GENERAL TOPOLOGY

The electrical circuit under study belongs to the type of feedback system shown in Fig. 1. The electrical circuit to be investigated will be established from this general configuration. This UDCF topology is distinguished by the fact that the direct chain transfer function is equal to unity. The feedback chain is generated via the subtraction of the main input and output. By denoting  $j\omega$  the angular frequency variable with  $j = \sqrt{-1}$ , the general input and output can be denoted  $V_i(j\omega)$  and  $V_o(j\omega)$ , respectively. The feedback voltage via the chain  $F(j\omega)$  must be equal to:

$$V_f(j\omega) = F(j\omega) \times V_o(j\omega). \quad (1)$$

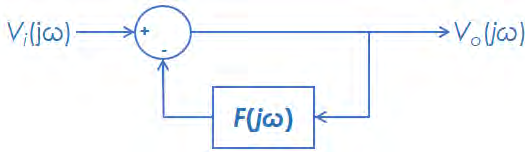


FIGURE 1. General topology of the UDCF system.

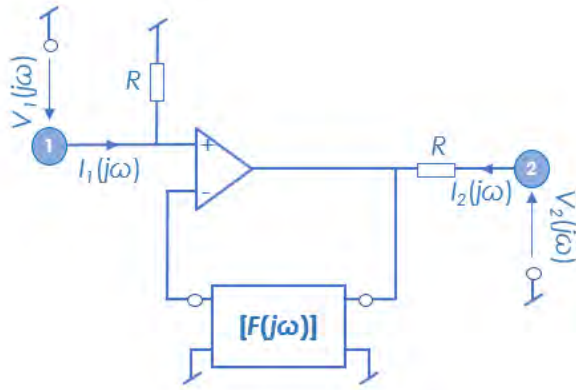


FIGURE 2. Amplifier operational-based UDCF general topology.

To realize the subtractor, we will use the classical circuit based on the operational amplifier. The following paragraph describes the analytical investigation of the UDCF based on this subtractor element.

**B. OPERATIONAL AMPLIFIER BASED FOUR-PORT FEEDBACK CHAIN TOPOLOGIES**

According to circuit theory, the feedback chain of the UDCF must be a passive system to increase the potential stability of the overall system. The UDCF system can be built using subtractor designed with the  $R$ -resistor parameter as shown in Fig. 2.

The resistors  $R$  serve to ensure the input and output access matching. To initiate the analytical process, the feedback system is assumed to be represented by a four-port chain as depicted in Fig. 2. It is worth to note that compared to the simple two-port network, the four-port feedback network enables to avoid the instability issue. The feedback chain can be characterized by the transfer matrix:

$$[F(j\omega)] = \begin{bmatrix} F_{11}(j\omega) & F_{12}(j\omega) \\ F_{21}(j\omega) & F_{22}(j\omega) \end{bmatrix}. \quad (2)$$

Different from the work proposed in [35], in the present paper, we suppose that the operational amplifier presents the voltage conversion gain as a frequency dependent quantity expressed as:

$$G(j\omega) = \frac{g}{1 + j\omega/\omega_0}. \quad (3)$$

The term  $g = G(\omega \approx 0)$  represents the DC gain and the term  $\omega_0$  is the 3-dB cut-off angular frequency.

**C. Z-MATRIX EXPRESSION**

Acting as two-port system, the impedance or Z-matrix is defined by:

$$[V(j\omega)] = [Z(j\omega)] [I(j\omega)] \\ \Rightarrow \begin{bmatrix} V_1(j\omega) \\ V_2(j\omega) \end{bmatrix} = \begin{bmatrix} Z_{11}(j\omega) & Z_{12}(j\omega) \\ Z_{21}(j\omega) & Z_{22}(j\omega) \end{bmatrix} \begin{bmatrix} I_1(j\omega) \\ I_2(j\omega) \end{bmatrix}. \quad (4)$$

The Z-matrix of the UDCF topology can be established from the basic principles of circuit theory. By taking into account the expressions defined in (2) and (3), we have:

$$[Z(j\omega)] = \begin{bmatrix} R & 0 \\ \frac{R \cdot F_{11}(j\omega)G(j\omega)}{F_{11}(j\omega) + G(j\omega)} & R \end{bmatrix}. \quad (5)$$

Note that  $[Z(j\omega)]$  is dependent only up to the first element of the feedback system matrix chain. The quantities  $F_{12}$ ,  $F_{21}$  and  $F_{22}$  do not affect the impedance matrix. The simplest lumped circuit able to generate the NGD function must be constituted by both resistor and capacitor elements. The following subsection develops the S-parameter analysis of this general topology.

**D. GENERAL S-PARAMETER OF THE NGD TOPOLOGY**

The S-parameter analysis developed in the present paper is performed with the reference impedance  $R_0 = 50 \Omega$  which can be calculated from the Z-to-S matrix transform. Consequently, the S-parameters can be calculated from the Z-matrix defined in (5) via the relationship:

$$[S(j\omega)] = \left\{ [Z(j\omega)] - \begin{bmatrix} R_0 & 0 \\ 0 & R_0 \end{bmatrix} \right\} \\ \times \left\{ [Z(j\omega)] + \begin{bmatrix} R_0 & 0 \\ 0 & R_0 \end{bmatrix} \right\}^{-1}. \quad (6)$$

Therefore, the S-parameters of the circuit presented in Fig. 2 can be expressed as:

$$[S(j\omega)] = \begin{bmatrix} S_{11}(j\omega) & S_{12}(j\omega) \\ S_{21}(j\omega) & S_{22}(j\omega) \end{bmatrix}, \quad (7)$$

with

- the isolation coefficient:

$$S_{12}(j\omega) = 0, \quad (8)$$

- the reflection coefficients:

$$S_{11}(j\omega) = S_{22}(j\omega) = \frac{R - R_0}{R + R_0}, \quad (9)$$

- and the transmission coefficient:

$$S_{21}(j\omega) = \frac{2R_0R G(j\omega)F_{11}(j\omega)}{G(j\omega) + F_{11}(j\omega)}. \quad (10)$$

Substituting the operational amplifier transfer function defined in (3), expression (10) becomes:

$$S_{21}(j\omega) = \frac{2R_0R g\omega_0 F_{11}(j\omega)}{(R_0 + R)^2 g\omega_0 + (\omega_0 + j\omega)F_{11}(j\omega)}. \quad (11)$$

The NGD from this transmittance analysis can be performed coefficient by calculating the associated group delay. Subsequently, the NGD existence condition can be formulated.

**E. MAGNITUDE, PHASE AND GROUP DELAY OF THE TRANSMISSION COEFFICIENT**

The magnitude of the previously defined transmission coefficient can be written as:

$$S_{21}(\omega) = |S_{21}(j\omega)| = \frac{2R_0R}{(R_0 + R)^2} \times \frac{N(\omega)}{D(\omega)} \quad (12)$$

with:

$$\begin{cases} N(\omega) = g\omega_0\sqrt{\Re [F_{11}(j\omega)]^2 + \Im [F_{11}(j\omega)]^2} \\ D(\omega) = \sqrt{[\omega_0(g + \Re [F_{11}(j\omega)]) - \omega\Im [F_{11}(j\omega)]]^2 + [\omega\Re [F_{11}(j\omega)] + \omega_0\Im [F_{11}(j\omega)]]^2} \end{cases} \quad (13)$$

where  $F_{11}(j\omega) = \Re [F_{11}(j\omega)] + j\Im [F_{11}(j\omega)]$ . The associated transmission phase:

$$\varphi(\omega) = \angle S_{21}(j\omega), \quad (14)$$

is defined by:

$$\varphi(\omega) = \arctan [\psi_n(\omega)] - \arctan [\psi_d(\omega)]. \quad (15)$$

by taking:

$$\begin{cases} \psi_n(\omega) = \frac{\Im [F_{11}(j\omega)]}{\Re [F_{11}(j\omega)]} \\ \psi_d(\omega) = \frac{\omega\Re [F_{11}(j\omega)] + \omega_0\Im [F_{11}(j\omega)]}{\omega_0(g + \Re [F_{11}(j\omega)]) - \omega\Im [F_{11}(j\omega)]} \end{cases} \quad (16)$$

The NGD analysis will be elaborated from the group delay definition:

$$\tau(\omega) = -\frac{\partial \varphi(\omega)}{\partial \omega} = \frac{\partial [\arctan [\psi_d(\omega)] - \arctan [\psi_n(\omega)]]}{\partial \omega} \quad (17)$$

The group delay is derived from the transmission phase via equation (15). For any real function  $\psi(\omega)$ , the calculation involves the following analytical derivation:

$$\frac{\partial \arctan [\psi(\omega)]}{\partial \omega} = \frac{\frac{\partial \psi(\omega)}{\partial \omega}}{1 + \psi^2(\omega)}. \quad (18)$$

This convention yields the following compact inequation of NGD existence conditions:

$$\left[1 + \psi_n^2(\omega)\right] \psi_n'(\omega) - \left[1 + \psi_d^2(\omega)\right] \psi_d'(\omega) > 0. \quad (19)$$

with:

$$\begin{cases} \psi_n'(\omega) = \frac{\partial \psi_n(\omega)}{\partial \omega} \\ \psi_d'(\omega) = \frac{\partial \psi_d(\omega)}{\partial \omega} \end{cases} \quad (20)$$

This condition can be explicitly rewritten as a function of the feedback chain parameters as:

$$\frac{\omega_0\Re [F_{11}(j\omega)]^4 + f_3\Re [F_{11}(j\omega)]^3 + f_2\Re [F_{11}(j\omega)]^2 + f_1\Re [F_{11}(j\omega)] + f_0}{\Re [F_{11}(j\omega)]^2 \left\{ \frac{\omega_0 [g + \Re [F_{11}(j\omega)]]}{-\omega\Im [F_{11}(j\omega)]} \right\}^2} > 0, \quad (21)$$

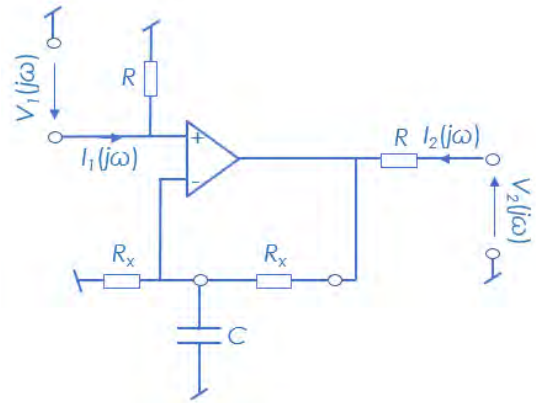


**FIGURE 3. UDCF NGD cell constituted by an amplifier operational in feedback with an  $R_x$  C-network.**

with:

$$\begin{cases} f_0 = \left\{ \frac{\Im [F_{11}(j\omega)]}{\Re [F_{11}(j\omega)]} \frac{\partial \Re [F_{11}(j\omega)]}{\partial \omega} \right. \\ \left. \left\{ \omega^2 \Im [F_{11}(j\omega)]^2 + 2\omega\omega_0g\Im [F_{11}(j\omega)] + g^2\omega_0^2 \right\} \right\} \\ f_1 = \left\{ 2\omega_0\Im [F_{11}(j\omega)] \left\{ \frac{\omega_0g}{+\omega\Im [F_{11}(j\omega)]} \right\} \frac{\partial \Re [F_{11}(j\omega)]}{\partial \omega} \right. \\ \left. + \left\{ \frac{2\omega\omega_0g\Im [F_{11}(j\omega)] - \omega^2\Im [F_{11}(j\omega)]^2 - \omega_0^2g}{\omega^2\Im [F_{11}(j\omega)]^2 + 2\omega\omega_0g\Im [F_{11}(j\omega)] + g^2\omega_0^2} \right\} \frac{\partial \Im [F_{11}(j\omega)]}{\partial \omega} \right\} \\ f_2 = \left\{ \frac{\omega_0\Im [F_{11}(j\omega)]^5}{+\omega_0\{2\omega\Im [F_{11}(j\omega)] + \omega_0g\}} \frac{\partial \Im [F_{11}(j\omega)]}{\partial \omega} \right. \\ \left. + \frac{\{\omega\omega_0g - \omega^2\Im [F_{11}(j\omega)]\}}{+\omega_0\{2\omega\Im [F_{11}(j\omega)] + \omega_0g\}} \frac{\partial \Re [F_{11}(j\omega)]}{\partial \omega} \right\} \\ f_3 = \omega_0g + \omega^2 \frac{\partial \Im [F_{11}(j\omega)]}{\partial \omega} \end{cases} \quad (22)$$

This NGD existence condition will be realized by using actual circuit parameters in the next section by focusing on the case of an RC-cell as the feedback network.

**III. NGD INVESTIGATION OF THE RC-CELL BASED TOPOLOGY**

As a concrete illustration of the previously described circuit theory, the present section is focused mainly on the NGD analysis of the RC cell-based feedback topology.

Fig. 3 represents the configuration of the UDCF topology to be developed in this paper. Clearly, the direct chain gain is equal to unity.

The feedback chain is constituted by the L-cell passive  $R_x$ C-network generated with the operational amplifier of the main input and output. The general input and output voltages can be denoted  $V1(j\omega)$  and  $V2(j\omega)$ , respectively. The access currents  $I1(j\omega)$  and  $I2(j\omega)$  are associated with port 1 (input) and port 2 (output), respectively. The resistance  $R_x$ , which is connected to the ground, is implemented to generate a positive gain. The resistors  $R$  serve to ensure the input and output access matching.

After a brief analytical definition of the constituting blocks of the topology, the analytical S-parameter modeling is described in the next paragraph.

**A. ANALYTICAL DEFINITION OF THE CONSTITUTING BLOCKS**

According to circuit theory, the feedback chain of the UDCF must be a passive system to increase the potential stability of the overall system. To initiate the analytical process, the feedback system is assumed to be represented by a four-port chain. It can be demonstrated that the  $R_x C$ -network feedback system presents the following transfer matrix:

$$[T(j\omega)] = \begin{bmatrix} T_{11}(j\omega) & T_{12}(j\omega) \\ T_{21}(j\omega) & T_{22}(j\omega) \end{bmatrix} = \begin{bmatrix} 1 + R_x Y(j\omega) & R_x \\ Y(j\omega) & 1 \end{bmatrix}, \quad (23)$$

with:

$$Y(\omega) = j\omega C + \frac{1}{R_x}. \quad (24)$$

**B. S-PARAMETER OF THE GENERAL TOPOLOGY**

The S-parameter analysis developed in the present subsection follows the same approach as that introduced in Subsection II-D.

Knowing the feedback chain transfer matrix, the Z-matrix of the UDCF topology depicted in Fig. 3 established from expression (5) is given by:

$$[Z(j\omega)] = \begin{bmatrix} R & 0 \\ \frac{R G(j\omega) [1 + R_x Y(j\omega)]}{1 + G(j\omega) + R_x Y(j\omega)} & R \end{bmatrix}. \quad (25)$$

As pointed out in the previous section, the reflection and isolation coefficients are the same as those introduced in (8) and (9). However, the transmission coefficient becomes:

$$S_{21}(j\omega) = \frac{\frac{2\omega_0 R_0 R g (2 + j\omega R_x C)}{(R_0 + R)^2}}{2j\omega + \omega_0 [2 + g + j\omega R_x C (\omega_0 + j\omega)]} = \frac{N_{rc}(j\omega)}{D_{rc}(j\omega)} \quad (26)$$

For the analytical clarity, let us take:

$$\begin{cases} N_{rc}(j\omega) = \frac{2\omega_0 R_0 R g (2 + j\omega R_x C)}{(R_0 + R)^2} \\ D_{rc}(j\omega) = \omega_0 (2 + g - \omega^2 R_x C) + j\omega (2 - \omega_0^2 R_x C). \end{cases} \quad (27)$$

The NGD analysis established from this transmittance coefficient by calculating the associated group delay will be discussed in the next subsection.

**1) MAGNITUDE, PHASE AND GROUP DELAY OF THE TRANSMISSION COEFFICIENT**

The magnitude of the previously defined transmission coefficient can be written as:

$$S_{21}(\omega) = |S_{21}(j\omega)| = \frac{|N_{rc}(j\omega)|}{|D_{rc}(j\omega)|}. \quad (28)$$

Accordingly, the corresponding magnitude is written as:

$$S_{21}(\omega) = \frac{\frac{2\omega_0 R_0 R g}{(R_0 + R)^2} \sqrt{4 + (\omega R_x C)^2}}{\sqrt{\omega_0^2 (2 + g - R_x C \omega^2)^2 + \omega^2 (2 + \omega_0 R_x C)^2}}. \quad (29)$$

The associated transmission phase is given by:

$$\varphi(\omega) = \arctan \left[ \frac{\text{Im}(N_{rc}(j\omega))}{\text{Re}(N_{rc}(j\omega))} \right] - \arctan \left[ \frac{\text{Im}(D_{rc}(j\omega))}{\text{Re}(D_{rc}(j\omega))} \right], \quad (30)$$

which will become:

$$\varphi(\omega) = \arctan \left( \frac{\omega R_x C}{2} \right) - \arctan \left[ \frac{\omega (2 + \omega_0 R_x C)}{\omega_0 (2 + g - R_x C \omega^2)} \right] \quad (31)$$

This equation implies the hereafter detailed formula of the UDCF cell group delay:

$$\tau(\omega) = \frac{\omega_0 \left[ \frac{R_x^4 C^4 \omega^4 + R_x^2 C^2 (8 + 6g + g R_x C \omega_0) \omega^2}{+ 2(2 + g)(4 - g R_x C \omega_0)} \right]}{(4 + R_x^2 C^2 \omega^2) \left[ \frac{R_x^2 C^2 \omega^4 + \omega_0^2 (g + 2)^2 + [4 + R_x C \omega_0 (R_x C \omega_0 - 2g)] \omega^2}{\omega^2} \right]}. \quad (32)$$

**2) STABILITY ANALYSIS**

The stability analysis can be performed in three different complementary ways.

*a: ANALYSIS 1*

First, the analysis of the transfer function represented by  $S_{21}$  is introduced. Next, with a system acting as a two-port circuit, the analysis based on the S-matrix via the Rollett stability factor is developed.

According to circuit and system theory, the proposed topology is unstable when the denominator of expression (26) is equal to zero. It implies the following equation system with the unknown  $\omega$ :

$$\begin{cases} \text{Re} \{ \text{denom} [S_{21}(j\omega)] \} = 0 \\ \text{Im} \{ \text{denom} [S_{21}(j\omega)] \} = 0, \end{cases} \quad (33)$$

which becomes:

$$\begin{cases} 2 + g - R_x C \omega^2 = 0 \\ 2 + R_x C \omega_0^2 = 0. \end{cases} \quad (34)$$

However, this equation system does not have any solution. Note that the expression of the transmission coefficient guarantees that the UDCF topology is conditionally stable.

*b: ANALYSIS 2*

The stability factor derived from the S-parameter defined as:

$$\mu(\omega) = \frac{1 - |S_{11}(j\omega)|^2}{|S_{12}(j\omega) S_{21}(j\omega) + \left| \begin{matrix} S_{22}(j\omega) - S_{11}^*(j\omega) \\ S_{11}(j\omega) S_{22}(j\omega) \\ -S_{12}(j\omega) S_{21}(j\omega) \end{matrix} \right|^2}} \quad (35)$$

with:

$$S_{11}^*(j\omega) = \text{conj}[S_{11}(j\omega)]. \quad (36)$$

By considering the S-parameters introduced in (7), this stability factor is transformed as:

$$\mu(\omega) = \frac{1}{|S_{11}(j\omega)|}, \quad (37)$$

which becomes:

$$\mu(\omega) = \frac{R + R_0}{|R - R_0|}. \quad (38)$$

It is note worthy that this quantity is obviously higher than unity:

$$\mu(\omega) > 1. \quad (39)$$

Moreover, the circuit proposed in Fig. 1 fulfills the stability necessary condition.

### c: ANALYSIS 3

The stability can also be defined from the matrix impedance [38]. By inverting the matrix defined in expression (25), we have the following admittance matrix:

$$[Y_n(j\omega)] = \begin{bmatrix} 1/R & 0 \\ \frac{\omega_0 g(2 + j\omega R_x C)/R}{\omega_0(1 + g) + j\omega(1 + R_x C \omega_0 g)} & 1/R \end{bmatrix}. \quad (40)$$

As introduced in [38], the proposed two-port analog circuit is stable under the following condition:

$$K(\omega) = \frac{2\Re[Y_{n1,1}(j\omega)]\Re[Y_{n2,2}(j\omega)] - \Re[Y_{n1,2}(j\omega)]\Re[Y_{n2,1}(j\omega)]}{|Y_{n1,2}(j\omega)Y_{n2,1}(j\omega)|} > 1. \quad (41)$$

The analytical calculation with the admittance matrix expressed in (40) gives  $K(\omega) = \infty$ . As a result, condition (41) is always respected and the circuit is unconditionally stable for any values of  $R, R_0, R_x$  and  $C$ .

### 3) NGD ANALYSIS

By aiming to establish the low-pass NGD, we must investigate the transmission coefficient magnitude and group delay at very low frequency  $\omega \approx 0$ . In this case, the magnitude of the UDCF cell transmission coefficient is given by:

$$|S_{21}(j\omega)|_{\omega=0} = \frac{4gR_0R}{(2 + g)(R_0 + R)^2}. \quad (42)$$

The group delay, at very low frequency  $\omega \approx 0$ , is written as:

$$\tau(0) = \tau(\omega)|_{\omega=0} = \frac{4 - R_x C \omega_0 g}{2\omega_0(2 + g)}. \quad (43)$$

Obviously, this quantity is negative under the following condition:

$$R_x C \omega_0 g > 4. \quad (44)$$

This inequation is equivalent to the following relationship between the  $R_x C$ -network and the operational amplifier parameters:

$$R_x C > (R_x C)_{\min} = \frac{4}{\omega_0 g}. \quad (45)$$

Thus, the UDCF cell can behaves as a low-pass NGD function. The NGD cut-off frequency (which is also the NGD bandwidth)  $\omega_c$  of the proposed UDCF cell is defined as the root of the equation:

$$\tau(\omega) = 0. \quad (46)$$

This condition implies the analytical solution:

$$\omega_c = \frac{\sqrt{g(2 + x)[32 + g(18 + x)] - 8 - 6g - gx}}{R_x C \sqrt{2}}, \quad (47)$$

with:

$$x = R_x C \omega_0. \quad (48)$$

This quantity can be rewritten as:

$$\omega_c = \frac{\sqrt{gx \sqrt{\left(1 + \frac{x}{2}\right) \left(1 + \frac{32+18g}{gx}\right)} - 8 - 6g - gx}}{R_x C \sqrt{2}}. \quad (49)$$

In the present study, we are focusing on the particular case of a low-pass NGD circuit built with the  $R_x C$ -network with:

$$\frac{1}{2\pi R_x C} < 10 \text{ MHz}, \quad (50)$$

and a high-speed operational amplifier:

$$\frac{\omega_0}{2\pi} > 1 \text{ GHz}. \quad (51)$$

By hypothesis, we may have the following relationship:

$$\frac{1}{R_x C \omega_0} = \frac{1}{x} \ll 1. \quad (52)$$

By implementing with the second order limited expansion with respect to  $1/x$ , we have:

$$\sqrt{\left(1 + \frac{x}{2}\right) \left(1 + \frac{32 + 18g}{gx}\right)} \approx 1 + \frac{2(8 + 5g)}{gx} + O\left(\frac{1}{x^2}\right). \quad (53)$$

Consequently, equation (34) can be approximated as:

$$\omega_c \approx \frac{\sqrt{gx \left[1 + \frac{2(8+5g)}{gx}\right] - 8 - 6g - gx}}{R_x C \sqrt{2}} = \frac{\sqrt{2(2 + g)}}{R_x C} \quad (54)$$

4) SYNTHESIS METHOD

Let us denote the targeted transmission gain, reflection coefficient, NGD level and NGD cut-off frequency as the following real variables respectively:

$$\begin{cases} g_{0dB} > 0 \\ r_{dB} < -10 \\ \tau(0) = \tau_0 < 0 \\ \omega_s \ll \omega_0, \end{cases} \quad (55)$$

The NGD synthesis method aims to determine the UDCF circuit that can fulfil these specifications. Indeed, this method consists of calculating the parameters  $R$ ,  $R_x$  and  $C$ , and the operational amplifier parameter  $g$  given the angular frequency  $\omega_0$ . The circuit parameters must be the roots of the equations below:

- input and output access matching:

$$S_{11}(\omega \approx 0) = S_{22}(\omega \approx 0) = r, \quad (56)$$

- transmission gain:

$$S_{21}(\omega \approx 0) = g_0, \quad (57)$$

- NGD level:

$$\tau(0) = \tau_0, \quad (58)$$

- and NGD bandwidth:

$$\omega_c = \omega_s. \quad (59)$$

a: SYNTHESIS OF R

The value of resistor  $R$  calculated from equation (56) is given by:

$$R = \frac{1+r}{1-r} R_0. \quad (60)$$

The value can also be calculated by inverting equation (57). In this case, the resistor  $R$  synthesis equation is given as follows:

$$R = \frac{2g - g_0(g+2) + 2\sqrt{g[g - g_0(g+2)]}}{g_0(g+2)} R_0. \quad (61)$$

It is found that this equation gives a realistic positive value only under the following condition:

$$g_0 < g_{0max} = \frac{g}{g+2}. \quad (62)$$

b: SYNTHESIS OF G

We can also determine the operational amplifier parameter  $g$  knowing the resistance  $R$ . In this case, by inverting equation (56), the following expression is obtained:

$$g = \frac{2g_0(R_0 + R)^2}{4R_0R - g_0(R_0 + R)^2}. \quad (63)$$

In this case, a realistic positive value is obtained from this last equation under the following condition:

$$g_0 < g_{0max} = \frac{4R_0R}{(R_0 + R)^2}. \quad (64)$$

Substituting expression (53) into (60), the expected gain can be rewritten in function of  $r$  as follows:

$$g = \frac{2g_0}{1 - g_0 - r^2}. \quad (65)$$

In this case, the desired reflection and transmission coefficients must verify the following condition:

$$g_0 < g_{0max} = 1 - r^2. \quad (66)$$

c: SYNTHESIS OF  $R_x C$

This quantity of the feedback chain parameters can be determined by inverting equations (55) or (59), yielding the following respective synthesis formulas:

$$R_x C = \frac{2[2 - \omega_0 \tau_0(2 + g)]}{\omega_0 g}, \quad (67)$$

$$R_x C \approx \frac{\sqrt{2(2 + g)}}{\omega_s}. \quad (68)$$

Combining the two equations, the relationship between the NGD level and cut-off frequency is established:

$$\omega_s \approx \frac{\omega_0 g \sqrt{2(2 + g)}}{2[2 - \omega_0 \tau_0(2 + g)]}. \quad (69)$$

It can be emphasized that the NGD level and NGD bandwidth are inversely proportional.

5) CHARACTERIZATION OF THE UDCF TOPOLOGY

The performance of the NGD topology depends especially on the NGD level and bandwidth. In addition to the microwave circuit performance, the NGD figure-of-merit (FoM) can be assessed with the formula:

$$FoM = \frac{\tau(\omega \approx 0) \omega_c S_{21}(\omega \approx 0)}{\sqrt{S_{11}(\omega \approx 0) S_{22}(\omega \approx 0)}}. \quad (70)$$

Knowing that,

$$S_{11}(\omega \approx 0) = S_{22}(\omega \approx 0), \quad (71)$$

this FoM can be simplified as:

$$FoM = \frac{S_{21}(\omega \approx 0)}{S_{11}(\omega \approx 0)} \tau(\omega \approx 0) \omega_c. \quad (72)$$

Considering the expressions of the reflection coefficient in (9), the transmission coefficient in (42), and the group delay in (43), the previous equation becomes:

$$FoM = \frac{4gR_0R\omega_c(4 - R_x C \omega_0 g)}{2\omega_0(2 + g)^2(R_0 + R) |R - R_0|}. \quad (73)$$

Substituting the approximate cut-off frequency introduced earlier, this FoM can be estimated as:

$$FoM = \frac{4g\sqrt{8 + 4g}R_0R(4 - \omega_0 g R_x C)}{2\sqrt{2}\omega_0(2 + g)^2 R_x C (R_0 + R) |R - R_0|}. \quad (74)$$

To verify the effectiveness of the theoretical investigation, simulation and experimental validation results will be discussed in the next section.

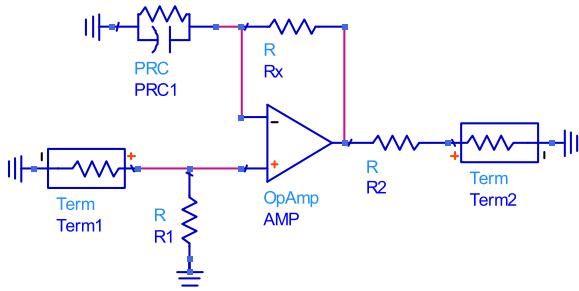


FIGURE 4. SPICE schematic of the ideal circuit simulated for the parametric analyses.

IV. SIMULATION AND EXPERIMENTAL VALIDATION RESULTS

As discussed in Section II, the NGD UDCF POC circuit can be designed. The design process is implemented in a manner similar to that of classical and familiar electronic analog circuits. To validate the NGD theory, parametric analyses as a function of the specified gain and NGD level are presented. The simulated and experimented results in both the frequency-domain and time-domain are discussed in this section.

A. PARAMETRIC ILLUSTRATIVE ANALYSES

The proposed numerical analyses aim to illustrate the relevance of the theoretical prediction. The relevant parameters are the desired gain  $g_0$  and the group delay  $\tau_0$  at very low frequency  $\omega \approx 0$ . They were determined by the synthesis method. The method consists of comparing the transmission coefficient and the group delay of the synthesized circuit. For these analyses, the specified input and output reflection coefficients are  $r = -20$  dB. It implies the matching resistor value, calculated from equation (59) is  $R = 61.1 \Omega$ . The maximum expected gain is  $g_{0max} = -0.087$  dB. The RC-network capacitor is fixed to 10 pF.

Two cases of S-parameter parametric simulations were performed from DC to 24 MHz. First, the parametric analyses were realized by varying the desired gain  $g_0$  from  $-1.2$  dB to  $-0.4$  dB for a fixed group delay, followed by varying the group delay  $\tau_0$  from  $-50$  ns to  $-20$  ns for a fixed gain. To do this, the S-parameters of the ideal circuit introduced in Fig. 4 were simulated. The numerical analyses were run in the ADS® schematic environment.

During the simulation, an ideal operational amplifier presenting conversion gain  $g$  and cut-off frequency  $f_0=1$  GHz was considered. Table 1 summarizes the calculated parameters of the ideal circuit. The table indicates the transmission gain and the RC-network resistance. The simulated transmission coefficients and group delays from different values of  $g_0$  and  $\tau_0$  are plotted in Fig. 5 and in Fig. 6, respectively. The proposed circuit is found to behave as a low-pass NGD function. As predicted in theory, inversely proportional to the transmission coefficient, the group delay absolute values decrease with  $R_x$ . However, the group delay absolute value increases with the operational amplifier gain  $g$ .

TABLE 1. Synthesized UDCF NGD Circuit Parameters Given the Expected Transmission Gain  $g_0$  and Group Delay  $\tau_0 < 0$ .

$g_0$	$\tau_0$	$g$	$R_x$	$R$	$C$
-1.2 dB	-40 ns	14.6	8.5 kΩ	61.1 Ω	10 pF
-1 dB		18			
-0.6 dB		32.9			
-0.3 dB		80.7			
-0.1 dB		1366			
-1 dB	-50 ns	18	10.6 kΩ		
	-40 ns		8.5 kΩ		
	-30 ns		6.38 kΩ		
	-20 ns		4.25 kΩ		
	-10 ns		2.13 kΩ		

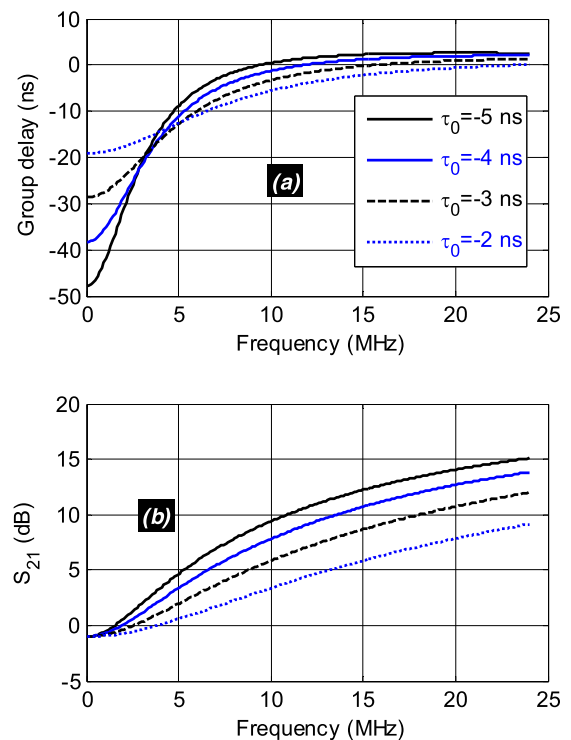


FIGURE 5. Parametric analysis results of the group delay and the transmission coefficient as a function of  $\tau_0$ .

To confirm this low-pass NGD function in a concrete manner, measurements versus simulations of a real prototype are discussed in the next paragraphs.

B. DESCRIPTION OF THE FABRICATED NGD PROTOTYPE

The optimized and normalized values of the implemented components were chosen to implement the real PCB. A prototype of a low-pass NGD active circuit was designed and fabricated as a POC. Fig. 7(a) shows a schematic of the designed NGD prototype.

As shown in Fig. 7(b), the prototype is a hybrid PCB designed with the packaged operational amplifier LMH6703 from Texas Instruments®. The size of the



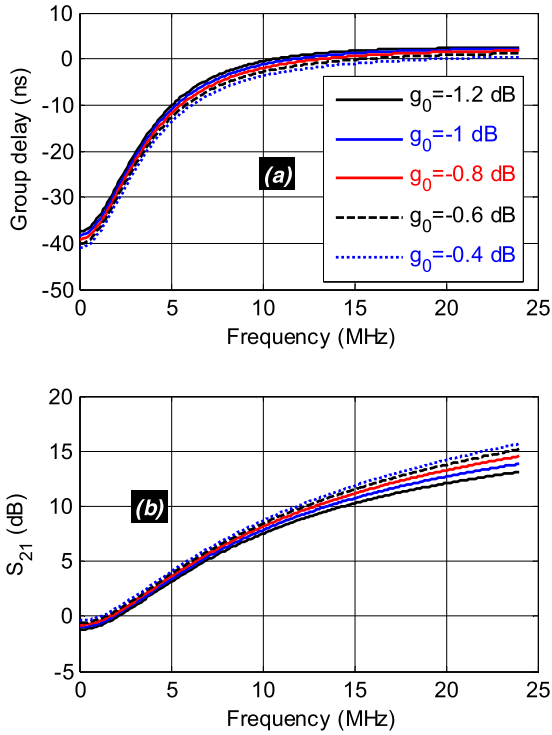


FIGURE 6. Parametric analysis results of the group delay and the transmission coefficient as a function of  $g_{0dB}$ .

TABLE 2. Fabricated NGD Circuit parameters.

Description	Parameters	Values	Tolerances
RC-network	$R_1$	8.2 k $\Omega$	5 %
	$R_2$	8.2 k $\Omega$	
	$C_1$	10 pF	
Matching resistance	$R_3$	62 $\Omega$	
	$R_4$	62 $\Omega$	
Bias network	$C_2$	100 nF	
	$C_3$	6.8 $\mu$ F	
	$C_4$	100 nF	
	$C_5$	6.8 $\mu$ F	

fabricated PCB is 30 mm  $\times$  40 mm. During the simulation, it is modeled with the ADS component presenting a conversion gain  $g = 30$  dB and cut-off frequency  $f_0 = 1$  GHz.

The considered operational amplifier was biased at  $V_{cc+} = +5$  V<sub>DC</sub> and  $V_{cc-} = -5$  V<sub>DC</sub> using a power supply. In addition to the NGD circuit RF part, the bias network includes the bypass capacitors.

Table 2 addresses the parameters of the fabricated NGD circuit prototype including the component tolerances.

### C. SIMULATED AND EXPERIMENTAL RESULTS

Frequency and time domain analyses were realized to illustrate the feasibility of the Low-pass NGD function with the proposed UDCF topology. The obtained results will be explored in the next paragraphs.

#### 1) FREQUENCY DOMAIN RESULTS

The present frequency analyses consist of comparing the transmission coefficient and the group delay from the simulated and measured S-parameters. The simulations are run

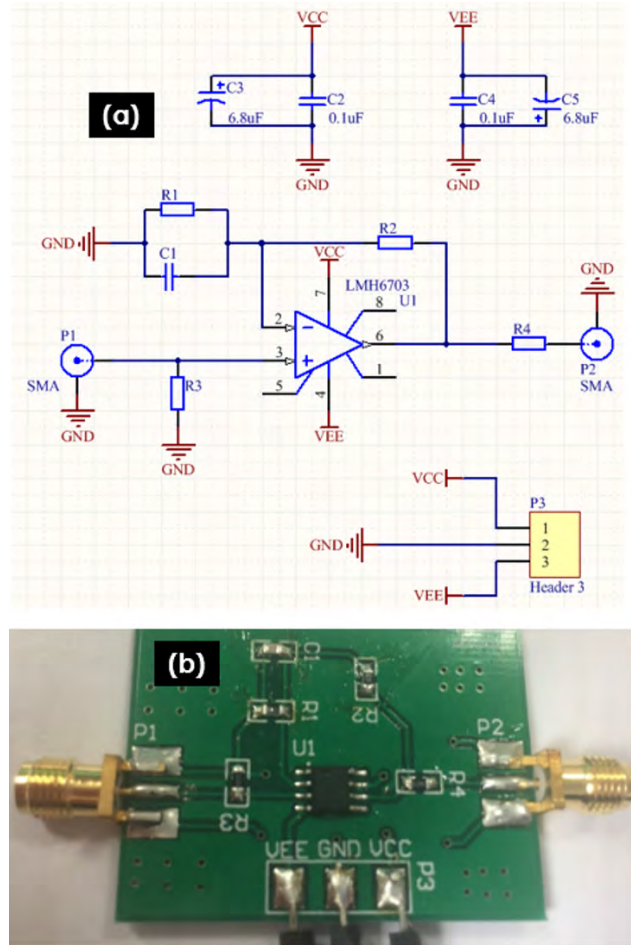


FIGURE 7. (a) Circuit design and (b) photograph of the tested NGD prototype.

in the ADS® environment of the electronic circuit designer and simulator generated from the prototype shown previously in Fig. 7. The S-parameter measurements are completed using a Vector Network Analyzer (VNA) from Rohde & Schwarz (ZNB 20, frequency band 100 kHz to 20 GHz). These frequency analyses are focused on the low frequency range from DC to 12 MHz.

Fig. 8(a) and Fig. 8(b) display comparisons of the simulated and measured transmission gain and phase. It is seen that the trends of simulation and measurement results are in good agreement. The high frequency deviation is explained by the difference between the operational amplifier model and the real one. Fig. 9 shows the correlation between the simulated and measured group delay responses.

It confirms the low-pass NGD behavior of the tested circuit. As expected, an NGD of approximately -38 ns appears at very low frequency. However, because of the fabrication imperfections and the operational amplifier unmatched model the simulated and measured NGD cut-off frequencies are different. It is worth to mention that the tested NGD circuit presents input and output reflection coefficients better than -15 dB in the NGD bandwidth. Moreover, the NGD

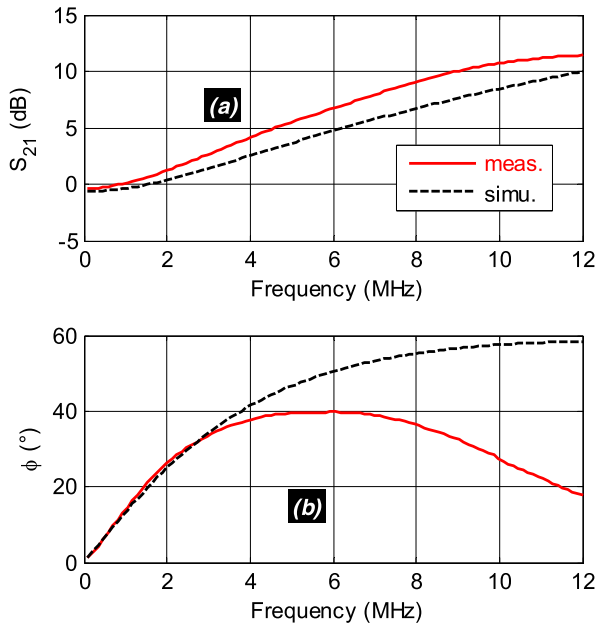


FIGURE 8. Comparisons between the simulated and measured transmission coefficient (a) magnitudes and (b) phases of the NGD prototype shown in Fig. 7.

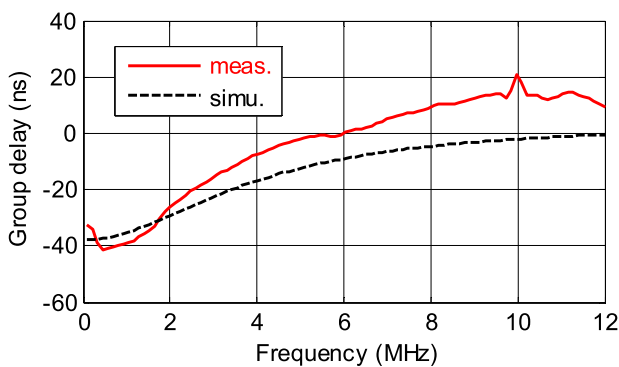


FIGURE 9. Comparisons between the simulated and measured group delay of the NGD prototype shown in Fig. 7.

TABLE 3. Comparison of band pass NGD circuit characteristics with the existing circuit available in [28], [29], [32].

References	$f_0$ (GHz)	$\tau_0$ (ns)	$\Delta f$ (MHz)	$S_{21}$ (dB)
[28]	1.30	-4.00	187	-20.00
[29]	1.79	-7.70	35	-8.60
[32]	0	-5	25	0
Proposed one	0	-38	6	0

prototype is unconditionally stable because the noise figure varies from 8.5 to 13.5 dB from DC to 0.1 GHz, i.e., noise figure is much higher than unity.

The proposed low-pass NGD prototype characteristics are compared with the existing circuits proposed in [28], [29] and [32]. As summarized in Table 3, the introduced NGD circuit presents a possibility to generate the most significant NGD absolute value. In addition to the design simplicity, it enables also to avoid the inherent losses.

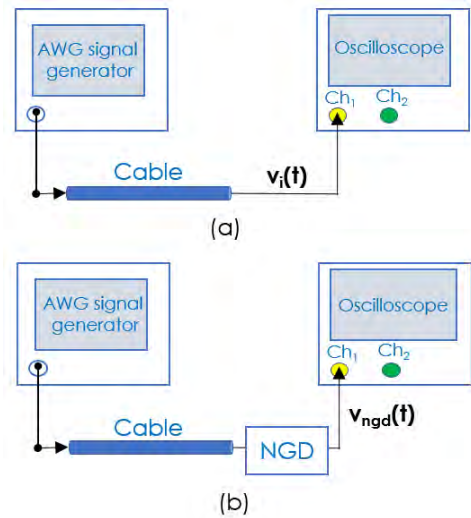


FIGURE 10. Illustrative diagram time-domain experimental setup: (a) input and (b) output signal measurements.

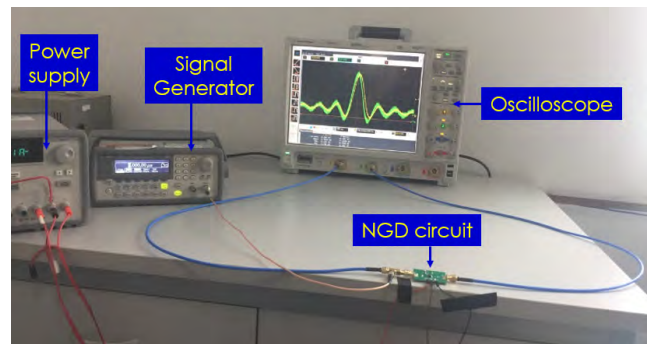


FIGURE 11. Photograph of the NGD time-domain experimental setup.

However, the NGD bandwidth is lower compared to the notably to the passive NGD circuits [32]. This bandwidth can be envisaged with cascaded several NGD cells.

## 2) TIME DOMAIN RESULTS

The time-domain validation aims to demonstrate the significance of the Low-pass NGD function. The validation consists of showing that the leading and trailing edges of the output voltage  $v_{out}(t)$  can be in advance compared to the input  $v_{in}(t)$ . As illustrated in Figs. 10, the time domain experimental validation is conducted by injecting pulse signal  $v_{in}$  to the tested NGD circuit.

During the test, the oscilloscope is configured to operate with input impedance  $R_0 = 50 \Omega$ . The tested signals are acquired by the oscilloscope through the T-SMA connector and SMA cables. During the tests, the input signal was provided by the arbitrary wave generator (AWG) referenced Agilent 33220A. As displayed in Fig. 9, the measured signals were visualized with the digital oscilloscope referenced Agilent DSO9404A having 4 GHz bandwidth and 20 Giga-sampling rate. For the present experimental study, the signal generator produces a typically sinc wave pulse signal that is a periodical signal having time-width of about 400 ns and

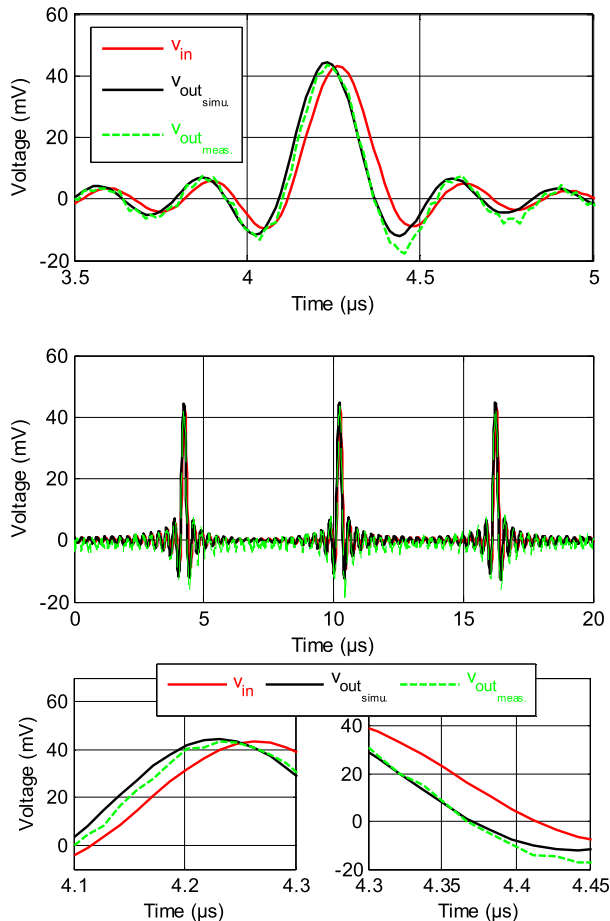


**FIGURE 12.** Transient simulated and measured results of the NGD prototype shown in Fig. 7. In bottom: Magnified view of the transient simulated and measured results of the NGD prototype shown in Fig. 7.

amplitude of approximately 45 mV. The recorded input and output transient signals  $v_{in}$  and  $v_{out}$ , respectively are plotted in Fig. 10. Despite the NGD effect, because of the circuit gain, the output signal amplitude presents an amplitude quite similar to the input. The plots of input and output voltages illustrate the evidence of time-advance.

Despite the SMA connector delay at the output port, as depicted in bottom of Fig. 12, the leading and trailing edges of the output signal  $v_{out}$  is of about 30 ns in advance of the input signal  $v_{in}$ . This outstanding time-advance explains the signature of the NGD effect. It can be realized with the low pass NGD circuit for the input signal with 90 % of power spectrum in the NGD bandwidth. Such NGD phenomenon can only appear with a smoothed signal. It is noteworthy that the NGD effect is not in contradiction with causality.

**D. TIME-DOMAIN DEMONSTRATION WITH A NON-PERIODIC AND SINGLE SHOT PULSE SIGNAL**

One may be concerned about the feasibility of the time-advance effect with non-periodical signals. To address this issue, a demonstration was carried out the results of which are described in the present subsection.

An innovative experiment based on non-periodic and non-repetitive signal was performed. To do this, a transient signal

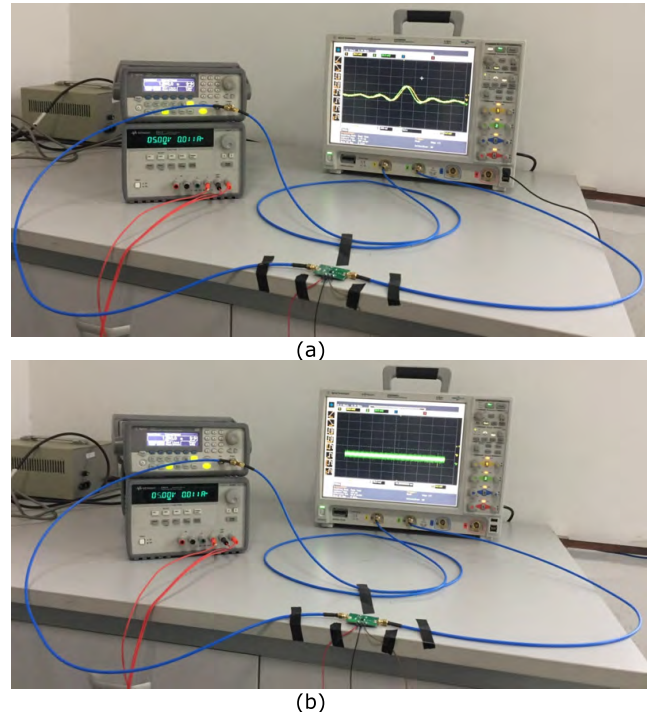


**FIGURE 13.** Photograph of the single shot pulse experimental results with time window visualization in (a) magnified view of range 200 ns and (b) in full scale range of 400 ms.

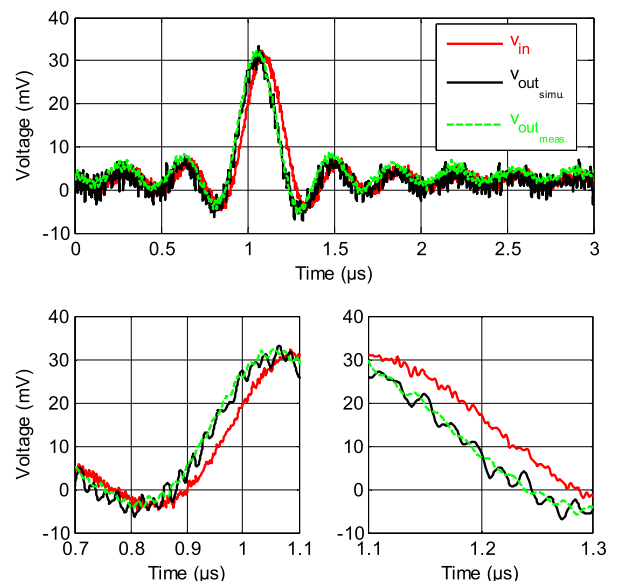


**FIGURE 14.** Time-domain measured results from the experimental setup shown in Fig. 13(a).

representing a single shot pulse was generated by using the internal burst function of an Agilent 33220A arbitrary wave generator (AWG). With this burst function, the signal generator output behaves as a single sinc waveform with a 400 ms time duration. The burst function is achieved by using trigger function. As shown in Fig. 13(a), the generator output was visualized by the oscilloscope as a sinc waveform after each trigger instant time detection.

The signal visualization was fixed after the single shot pulse recording by stopping the generator. This test pulse is generated without changing the other AWG parameters. The full-scale range of the non-periodic experimental test with no repetition of sequence is shown in Fig. 13(b). Note that, with this 400 ms time window, only one single pulse is visible corresponding to the generated AWG burst. As illustrated by the 200 ns time window visualization of Fig. 14, the NGD circuit output is earlier than the non-periodic single pulse input.

Clearly, there is significant integrity between the input and output signal waveforms. In a nutshell, the developed NGD circuit operates with a time advance without anti causal aspect.

## V. CONCLUSION

An innovative NGD theory of an active circuit was developed. The NGD topology used involves an UDCF cell implemented with an operational amplifier and RC-network circuit. The theoretical study was based on S-parameter modeling that includes the stability analysis via the Rollett factor. The NGD analysis as a function of the proposed UDCF cell parameters was established. The appearance of the instability as a function of the operational amplifier bandwidth was investigated. The proposed synthesis design method allows one to determine the circuit parameters as a function of the targeted NGD is proposed.

The feasibility of the NGD theory was verified by the fabrication of a POC circuit prototype. First, parametric analyses highlighted the verification of the NGD synthesis method. Then, the simulated and measured S-parameters confirmed the generation of NGD up to some Mega-Hertz. Similar to an all active circuit, the proposed NGD topology presents a capacity to operate with gain, matching and stability.

In the future, the developed NGD concept can be prominent for the enhancement of electronic circuits and systems. The NGD low-pass, high-pass and bandpass circuits are future potential candidates for use in the correction of signal delays as propagation RC effects [37].

## REFERENCES

- [1] Q.-K. Li and H. Lin, "Effects of mixed-modes on the stability analysis of switched time-varying delay systems," *IEEE Trans. Autom. Control*, vol. 61, no. 10, pp. 3038–3044, Oct. 2016.
- [2] C.-K. Zhang, Y. He, L. Jiang, M. Wu, and H.-B. Zeng, "Delay-variation-dependent stability of delayed discrete-time systems," *IEEE Trans. Autom. Control*, vol. 61, no. 9, pp. 2663–2669, Sep. 2016.
- [3] J. Shen and J. Lam, "Stability and performance analysis for positive fractional-order systems with time-varying delays," *IEEE Trans. Autom. Control*, vol. 61, no. 9, pp. 2676–2681, Sep. 2016.
- [4] W. Pasillas-Lépine, A. Loria, and T.-B. Hoang, "A new prediction scheme for input delay compensation in restricted-feedback linearizable systems," *IEEE Trans. Autom. Control*, vol. 61, no. 11, pp. 3693–3699, Nov. 2016.
- [5] W. Xiang, "Necessary and sufficient condition for stability of switched uncertain linear systems under dwell-time constraint," *IEEE Trans. Autom. Control*, vol. 61, no. 11, pp. 3619–3624, Nov. 2016.
- [6] K. Shujaee and B. Lehman, "Vibrational feedback control of time delay systems," *IEEE Trans. Autom. Control*, vol. 42, no. 11, pp. 1529–1545, Nov. 1997.
- [7] E. Fridman and U. Shaked, "An improved stabilization method for linear time-delay systems," *IEEE Trans. Autom. Control*, vol. 47, no. 11, pp. 1931–1937, Nov. 2002.
- [8] L. Liu, G. Zhang, W. Li, and Z. Zuo, "Delay-dependent H-infinity control of linear descriptor systems," in *Proc. 7th World Congr. Intell. Control Automat.*, Chongqing, China, Jun. 2008, pp. 1390–1395.
- [9] M. Wu, Y. He, J.-H. She, and G.-P. Liu, "Delay-dependent criteria for robust stability of time-varying delay systems," *Automatica*, vol. 40, no. 8, pp. 1435–1439, 2004.
- [10] K. Gu, "An integral inequality in the stability problem of time-delay systems," in *Proc. 39th IEEE Conf. Decis. Control*, Sydney, NSW, Australia, Dec. 2000, pp. 2805–2810.
- [11] E. C. Heyde, "Theoretical methodology for describing active and passive recirculating delay line systems," *Electron. Lett.*, vol. 31, no. 23, pp. 2038–2039, Nov. 1995.
- [12] G. Groenewold, "Noise and group delay in active filters," *IEEE Trans. Circuits Syst. I, Reg. Papers*, vol. 54, no. 7, pp. 1471–1480, Jul. 2007.
- [13] C. Wijenayake, Y. Xu, A. Madanayake, L. Belostotski, and L. T. Bruton, "RF analog beamforming fan filters using CMOS all-pass time delay approximations," *IEEE Trans. Circuits Syst. I, Reg. Papers*, vol. 59, no. 5, pp. 1061–1073, May 2012.
- [14] D. Solli, R. Y. Chiao, and J. M. Hickmann, "Superluminal effects and negative group delays in electronics, and their applications," *Phys. Rev. E, Stat. Phys. Plasmas Fluids Relat. Interdiscip. Top.*, vol. 66, pp. 056601-1–056601-4, Nov. 2002.
- [15] M. W. Mitchell and R. Y. Chiao, "Negative group delay and 'fronts' in a causal system: An experiment with very low frequency bandpass amplifiers," *Phys. Lett. A*, vol. 230, pp. 133–138, Jun. 1997.
- [16] M. W. Mitchell and R. Y. Chiao, "Causality and negative group delays in a simple bandpass amplifier," *Amer. J. Phys.*, vol. 66, no. 1, pp. 14–19, 1998.
- [17] T. Nakanishi, K. Sugiyama, and M. Kitano, "Demonstration of negative group delays in a simple electronic circuit," *Amer. J. Phys.*, vol. 70, no. 11, pp. 1117–1121, 2002.
- [18] M. Kitano, T. Nakanishi, and K. Sugiyama, "Negative group delay and superluminal propagation: An electronic circuit approach," *IEEE J. Sel. Topics Quantum Electron.*, vol. 9, no. 1, pp. 43–51, Jan./Feb. 2003.
- [19] N. S. Bukhman and S. V. Bukhman, "On the negative delay time of a narrow-band signal as it passes through the resonant filter of absorption," *Radiophysics Quantum Electron.*, vol. 47, no. 1, pp. 66–76, Jan. 2004.
- [20] J. N. Munday and R. H. Henderson, "Superluminal time advance of a complex audio signal," *Appl. Phys. Lett.*, vol. 85, no. 3, pp. 503–505, Jul. 2004.
- [21] J. N. Munday and W. M. Robertson, "Observation of negative group delays within a coaxial photonic crystal using an impulse response method," *Opt. Commun.*, vol. 273, no. 1, pp. 32–36, 2007.
- [22] H. U. Voss, "Signal prediction by anticipatory relaxation dynamics," *Phys. Rev. E, Stat. Phys. Plasmas Fluids Relat. Interdiscip. Top.*, vol. 93, Mar. 2016, Art. no. 030201(R).
- [23] H. U. Voss, "A simple predictor based on delay-induced negative group delay," 2016, *arXiv:1606.07791*. [Online]. Available: <https://arxiv.org/abs/1606.07791>
- [24] H. U. Voss, "The leaky integrator with recurrent inhibition as a predictor," *Neural Comput.*, vol. 28, no. 8, pp. 1498–1502, Aug. 2016.
- [25] H. U. Voss and N. Stepp, "A negative group delay model for feedback-delayed manual tracking performance," *J. Comput. Neurosci.*, vol. 41, no. 3, pp. 295–304, 2016.
- [26] M. Kandic and G. E. Bridges, "Asymptotic limits of negative group delay in active resonator-based distributed circuits," *IEEE Trans. Circuits Syst. I, Reg. Papers*, vol. 58, no. 8, pp. 1727–1735, Aug. 2011.
- [27] M. Kandic and G. E. Bridges, "Limits of negative group delay phenomenon in linear causal media," *Prog. Electromagn. Res.*, vol. 134, pp. 227–246, 2013.
- [28] O. F. Siddiqui, M. Mojahedi, and G. V. Eleftheriades, "Periodically loaded transmission line with effective negative refractive index and negative group velocity," *IEEE Trans. Antennas Propag.*, vol. 51, no. 10, pp. 2619–2625, Oct. 2003.
- [29] G. Liu and J. Xu, "Compact transmission-type negative group delay circuit with low attenuation," *Electron. Lett.*, vol. 53, no. 7, pp. 476–478, Mar. 2017.
- [30] B. Ravelo, "Innovative theory on multiband NGD topology based on feedback-loop power combiner," *IEEE Trans. Circuits Syst. II, Exp. Briefs*, vol. 63, no. 8, pp. 738–742, Aug. 2016.

- [31] B. Ravelo, "Methodology of elementary negative group delay active topologies identification," *IET Circuits Devices Syst.*, vol. 7, no. 3, pp. 105–113, May 2013.
- [32] F. Wan, N. Li, B. Ravelo, Q. Ji, B. Li, and J. Ge, "The design method of the active negative group delay circuits based on a microwave amplifier and an RL-series network," *IEEE Access*, vol. 6, pp. 33849–33858, Jun. 2018.
- [33] F. Wan, N. Li, B. Ravelo, J. Ge, and B. Li, "Time-domain experimentation of NGD active RC-network cell," *IEEE Trans. Circuits Syst. II, Exp. Briefs*, vol. 66, no. 4, pp. 562–566, Apr. 2019.
- [34] B. Ravelo, "Similitude between the NGD function and filter gain behaviours," *Int. J. Circuit Theory Appl.*, vol. 42, no. 10, pp. 1016–1032, Oct. 2014.
- [35] B. Ravelo, "Theory on negative time-delay looped system," *IET Circuits, Devices Syst.*, vol. 12, no. 2, pp. 175–181, Mar. 2018.
- [36] B. Ravelo, "Unity direct chain with feedback series impedance based innovative negative group delay circuit," *Int. J. Electron. Commun.*, vol. 91, pp. 11–17, Jul. 2018.
- [37] P. K. Chan and M. D. F. Schlag, "Bounds on signal delay in RC mesh networks," *IEEE Trans. Comput.-Aided Des. Integr. Circuits Syst.*, vol. 8, no. 6, pp. 581–589, Jun. 1989.
- [38] M. A. Niknejad. Power gain and stability. Lecture, Univ. Berkeley, 2018. [Online]. Available: [http://rfic.eecs.berkeley.edu/ee242/pdf/Module\\_3\\_2\\_GainStability.pdf](http://rfic.eecs.berkeley.edu/ee242/pdf/Module_3_2_GainStability.pdf)



**FAYU WAN** received the Ph.D. degree in electronic engineering from the University of Rouen, Rouen, France, in 2011. From 2011 to 2013, he was a Postdoctoral Fellow with the Electromagnetic Compatibility Laboratory, Missouri University of Science and Technology, Rolla. He is currently a Full Professor with the Nanjing University of Information Science and Technology, Nanjing, China. His current research interests include negative group delay circuits, electrostatic discharge,

electro-magnetic compatibility, and advanced RF measurement.



**TAOCHENG GU** received the B.Sc. degree in electrical engineering from the Nanjing University of Information Science and Technology, Nanjing, China, in 2018, where he is currently pursuing the M.S. degree. His research interests include abnormal wave propagation in dispersive media and microwave circuits.



**BLAISE RAVELO** received the Ph.D. degree from the University of Brest, in 2008, and the Habilitation à Diriger des Recherches (HDR) degree from the University of Rouen, France, in 2012, where he led his HDR dissertation research. He is currently an Associate Professor with the Graduate Engineering School ESIGELEC/IRSEEM, Rouen. He is also a pioneer of the negative group delay (NGD) RF/analog and digital circuits, and systems. He has coauthored more than 200 papers and regularly

involved in national/international research projects. He co-supervised and directed nine Ph.D. students and six Ph.D. candidates who defended. He participates regularly in large Research and Development international projects. His current publication H-index is 16 (Reference: Google Scholar 2017). His research interests include microwave circuit design, electromagnetic compatibility (EMC) and interference (EMI), and signal and power integrity (SI/PI) engineering.

Dr. Ravelo has been a URSI member and is a member of Advanced Electromagnetic Symposium 2013–2018 technical committee and a member of the IEEE RADIO 2015 scientific committee. He is the Scientific Chair of the 5th International Conference on Electromagnetic Near Field Characterization and Imaging in 2011. He is regularly invited to review papers submitted to international journals (the IEEE TMTT, IEEE ACCESS, the IEEE TCS, the IEEE TEMC, the IEEE TIM, the IEEE TIE, the *Journal of Electromagnetic Waves and Applications*, the IET CDS, the IET MAP, and the International Journal of Electronics.) and international books (Wiley and Intech Science.)



**BINHONG LI** received the M.S. degree in Micro and Nanoelectronics from the University of Grenoble, France, in 2008, and the Ph.D. degree in EMC and reliability of ICs from the Institut Nationale des Sciences Appliquees (INSA), Toulouse, France, in 2011. He is currently an Associate Professor of SOI circuit and device reliability and EMC with the Institute of Microelectronics, Chinese Academy of Sciences (IMECAS), Beijing, China, where he was appointed in 2012.



**JING CHENG** received a Ph.D. degree in mathematics from the Shanghai Normal University, Shanghai, China, in 2010. She is currently an Associate Professor at Anhui Agricultural University, Hefei, China. Her current research interests include linear model, experimental and analysis.



**QINGYUN YUAN** received the B.S. degree in computer application, the M.S. and Ph.D. degrees in electromagnetic field and microwave technology from Mechanical Engineering College, Shijiazhuang, China, in 2003, 2006, and 2010, respectively. He is currently a Lecturer with Army Engineering University of PLA, Shijiazhuang, China. His research interests include electrostatic discharge (ESD) test and electromagnetic compatibility (EMC).



**JUNXIANG GE** received the Ph.D. degree in radio engineering from the Southeast University, Nanjing, China, in 1991. He has been the Dean of the School of Electronic and Information Engineering, Nanjing University of Information Science and Technology, Nanjing, since 2011. His current research interests include electromagnetic field theory, microwave and millimeter wave technology, and antenna.

...